Turkish Journal of Chemistry

http://journals.tubitak.gov.tr/chem/

Research Article

Turk J Chem
(2015) 39: 813 – 823

doi:10.3906/kim-1501-30

Enhanced electrocatalytic efficiency of C/MWNTs for methanol oxidation using Ni deposited on MWNTs

Murat FARSAK[1,2,*], **Gülfeza KARDAŞ**[2]

[1]Department of Chemistry, Faculty of Science and Letters, Osmaniye Korkut Ata University, Osmaniye, Turkey
[2]Department of Chemistry, Faculty of Science and Letters, Çukurova University, Adana, Turkey

Received: 12.01.2015 • **Accepted/Published Online:** 20.04.2015 • **Printed:** 28.08.2015

Abstract: The power density of direct methanol fuel cells (DMFCs) can be changed by using different anode materials. Especially porous materials are preferred for the anode. In the present study, multiwall carbon nanotubes were first injected into graphite. Then, by depositing nickel, a catalyst was prepared for use as the anode material of the DMFC. This catalyst was named Ni@MWNTs. The oxidation of methanol and some kinetic parameters were investigated in KOH solution. Cyclic voltammetry was used for the electrochemical measurements. Kinetic parameters of the methanol oxidation were determined at different temperatures, scan rates, and concentrations of methanol. The surface morphologies and nickel deposition amounts of the Ni@MWNTs and Ni-C (nickel deposited graphite) electrodes were characterized with scanning electron microscope (SEM), atomic force microscope (AFM), and energy-dispersive X-ray (EDX) spectroscope. It was found that the Ni@MWNTs electrode was more active than the Ni-C electrode. The activation energy of the Ni@MWNTs electrode was calculated as 19.52 kJ mol^{-1} for the methanol oxidation process.

Key words: Fuel cells, nanostructured materials, catalyst, composite materials, anode

1. Introduction

In recent times, the search for alternative energy sources has increased with developing technology. Lithium ion batteries, often used in electrical devices, have become inadequate. In Figure 1, a Ragone plot shows the practical energy and power density diagram of developing energy storage technologies.[1,2] Investigations of the fuel cell are gaining impetus. One of the most important systems is direct methanol fuel cells (DMFCs), whose advantages are low pollutant emission, low operating temperature, and high theoretical energy density of methanol (6.1 Wh g^{-1}). However, there are several problems in the commercialization of DMFCs, such as poisoning of electroactive sites with intermediate species and low kinetics of the methanol oxidation reaction (MOR).[3] It has been considered that transition metals or oxides may enhance the electrocatalytic stability and activity and reduce the costs of DMFCs.[4]

One of the transition metals used in DMFCs is nickel. This is because of its excellent oxidation properties. Nickel is utilized as an electrocatalyst in both anodic and cathodic reactions in organic synthesis and water electrolysis.[5–8] Recently, nickel-based electrode materials have been used as catalysts or components of catalysts because of their various electrochemical reactions. Other significant features of nickel-based electrodes are as follows: they show good stability in alkaline media, reduce costs, and improve kinetics in excessive

*Correspondence: muratfarsak@osmaniye.edu.tr

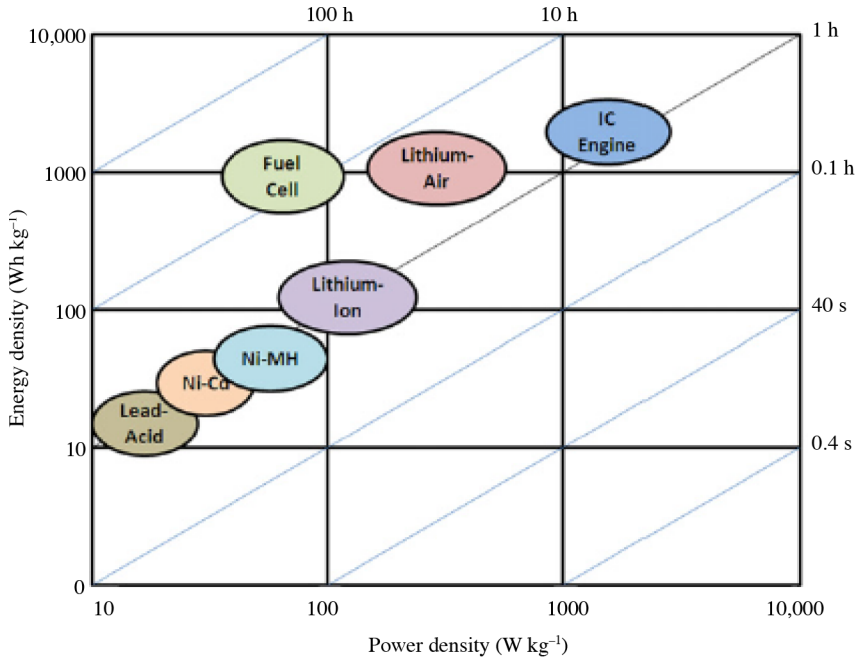

Figure 1. Ragone plot comparing the practical energy and power densities of current developing energy storage technologies with the fuel cells.

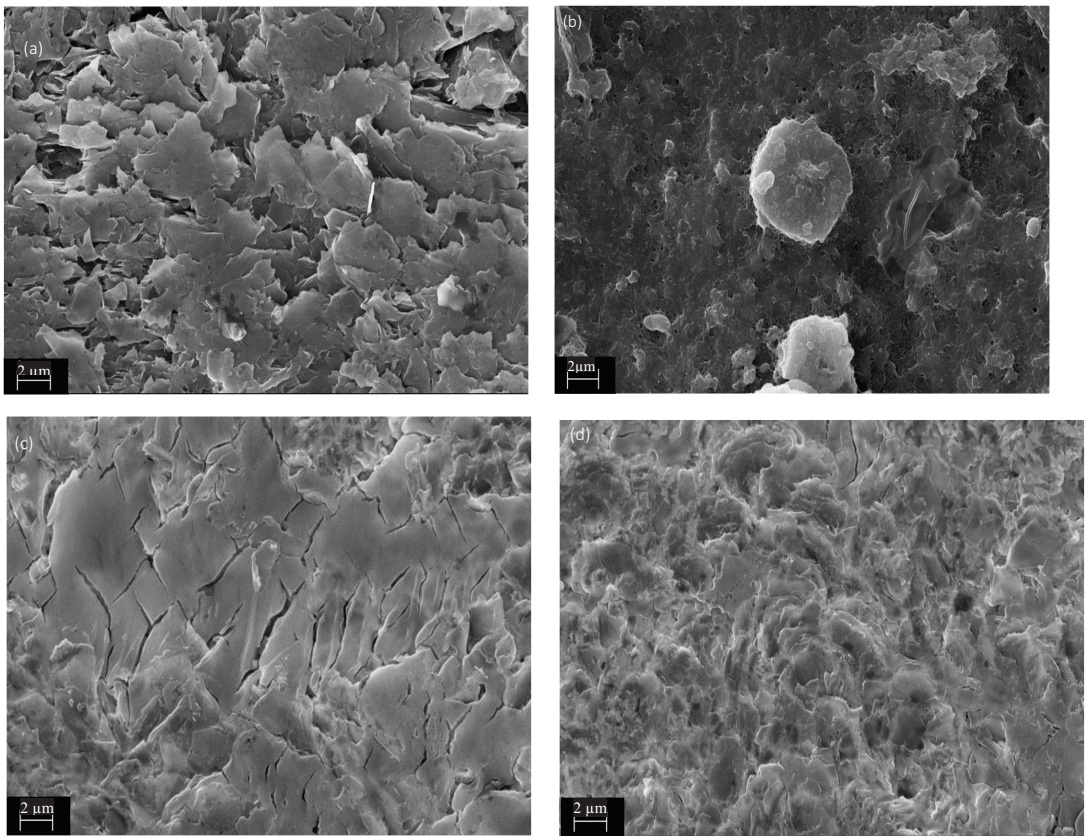

Figure 2. SEM images of C (a), C/MWNTs (b), C-Ni (c), and Ni@MWNTs (d) electrodes (mag: 5.00 kx).

acidic solutions.[9] Moreover, it has been found that nickel shows excellent efficiency in the electrooxidation of alcohols.[10–12]

One of the most important factors in electrooxidation is the surface area of catalysts. Thus catalysts can show high electrocatalytic activity if they have a large surface area. Carbon nanotubes (CNTs) possess some important features including large surface area, low resistance, high stability,[13–15] and authentic chemical and physical properties. In the literature there are two types of carbon nanotubes: single-wall carbon nanotubes (SWNTs) and multiwall carbon nanotubes (MWNTs). Enhanced electrocatalysts for low-temperature fuel cells have been monitored on both SWNTs and MWNTs.[16] When MWNTs were used as a support material for Pt-based electrocatalysts, the electrocatalytic activities were increased for both the oxygen reduction at the cathode[17] and the oxidation of CO[18] and methanol[19–21] at the anode.

The present study was carried out in order to determine the electrocatalytic efficiency of Ni@MWNTs as an anodic electrocatalyst in methanol electrooxidation. The results obtained show that Ni@MWNTs as electrocatalyst improve the stability and catalytic activity in the MOR.

2. Results and discussion

2.1. Characterization

As seen in Figure 2a, the surface of the graphite electrode had microleaves. These microleaves were closed by MWNTs, which had a fibrous structure (Figure 2b). When Ni was deposited on graphite, cracks were seen on the surface instead of microleaves (Figure 2c). The SEM image of the Ni@MWNTs electrode shows that microleaves were covered by a fibrous structure. In addition, metallic Ni particles are seen in the fibrous zone in Figure 2d. All SEM images were obtained under the same conditions (magnitude: 5.00 kx and 2 μm).

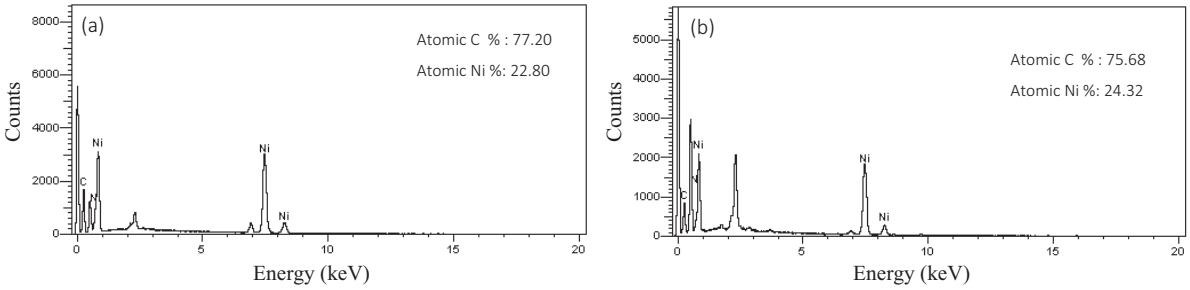

Figure 3. EDX spectra of Ni-C (a) and Ni@MWNTs (b) layers.

Figure 3 demonstrates that the percentages of atomic nickel amounts are 22.80% and 24.32% on Ni-C (Figure 3a) and Ni@MWNTs (Figure 3b) electrodes, respectively. They have the same deposition time.

Figures 4a and 4b show 2D and 3D AFM images of Ni-C, while Figures 4c and 4d show 2D and 3D AFM images of Ni@MWNTs electrodes, respectively. Small islets and slits are observed on the Ni@MWNTs surface. It could be associated with the large surface area and higher catalytic efficiency for methanol electrooxidation.

2.2. Nickel deposition on the C/MWNTs electrode

Figure 5 illustrates the effect of nickel deposition (at 50, 80, 100, 200, and 300 s) on electrooxidation of 0.50 M methanol in 1.00 M KOH at the C/MWNTs electrode at the scan rate of 100 mV s^{-1}. The deposition times of nickel on the surface of the C/MWNTs, the current densities, and the potentials of methanol oxidation for the Ni@MWNTs catalysts are given in the Table. The highest oxidation peak potential and peak current

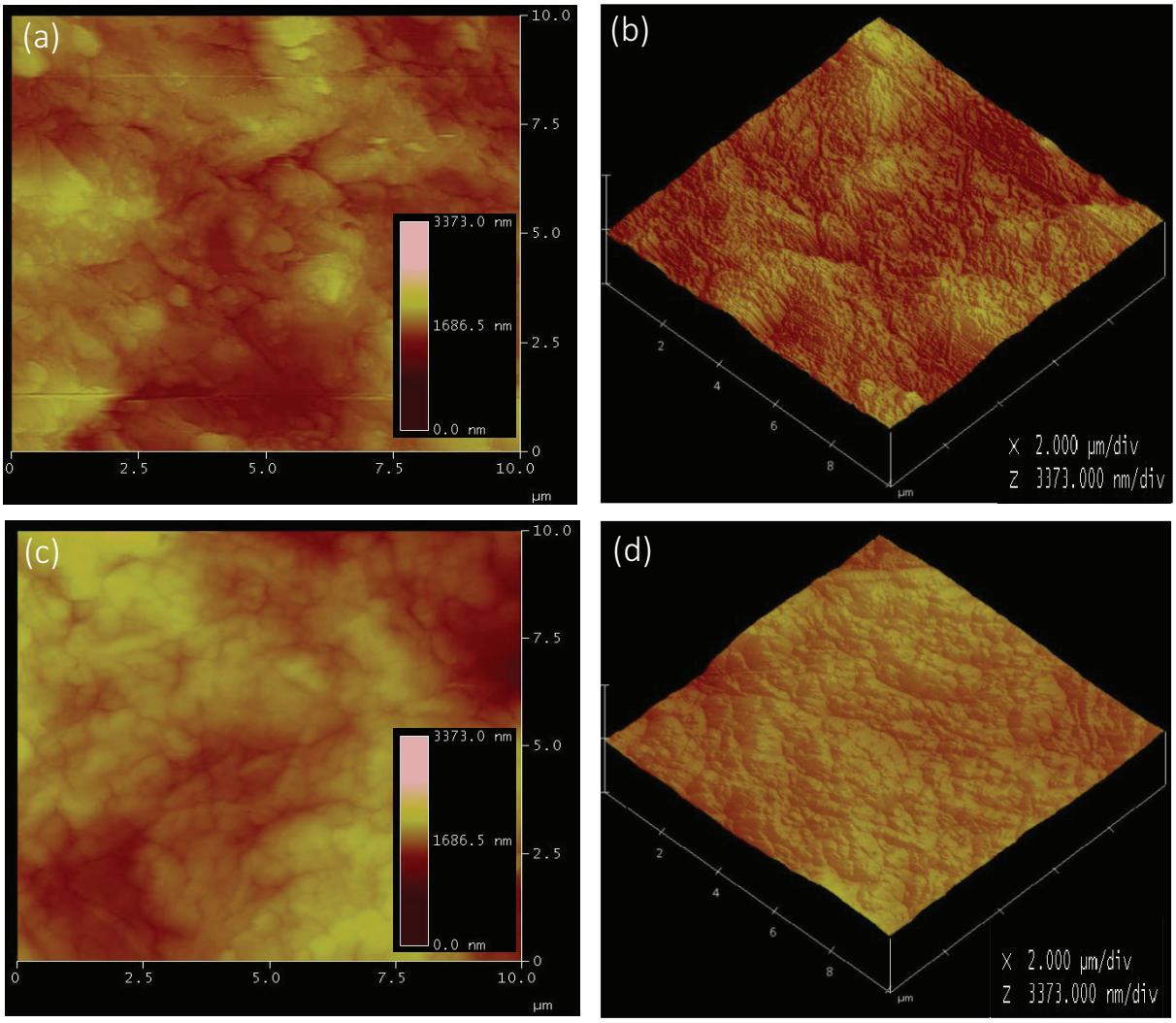

Figure 4. 2D, 3D AFM images of C-Ni (a) and (b), Ni@MWNTs (c) and (d).

density were obtained at 80 s of nickel deposition according to the Table. As seen in the Table, nickel deposition times affected methanol oxidation. In general, the current density decreased when a high amount of nickel was deposited. The reason for this was that the increasing amount of nickel decreased the porosity of the surface. Moreover, it could have closed the active regions. As a result of nickel deposition, a thin film formed on the surface. Excessive amounts of nickel deposition may cause loss of mechanical properties,[22−24] so that electron transfer may become difficult.[25]

2.3. Ni@MWNTs

Cyclic voltammograms were obtained using C, C/MWNTs, C-Ni, and Ni@MWNTs catalysts in 1.00 M methanol containing 1.00 M KOH solution at 100 mV s^{-1} scan rate, and they can be seen in Figure 6. C and C/MWNTs have no oxidation peak in the MOR. When nickel was deposited on their surfaces, both catalysts also showed good efficiency in the MOR. The Ni@MWNTs catalyst was more effective than the C-Ni catalyst for methanol oxidation due to the presence of MWNTs, which form a larger surface and a porous structure. In addition, oxidation current density of nickel redox couples of the Ni@MWNTs catalyst was higher than that of C-Ni.

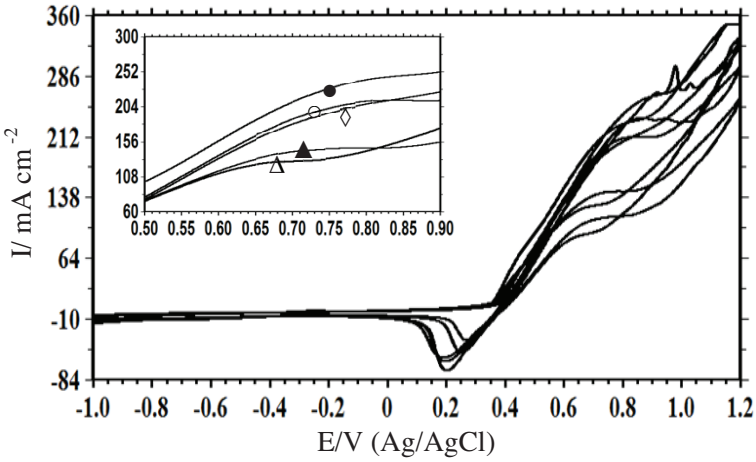

Figure 5. Effect of the different Ni deposition times (○) 50; ●) 80; ◇) 100; ▲) 200; Δ) 300 s on the electrooxidation of 0.50 M CH_3OH in 1.00 M KOH for Ni@MWNTs electrode at 298 K.

Table. Oxidation potential and current density for different deposition periods.

Periods	50	80	100	200	300
E_{Ox} vs. Ag/AgCl (V)	0.795	0.798	0.791	0.733	0.671
I_{Ox} (mA cm^{-2})	0.206	0.228	0.210	0.145	0.127

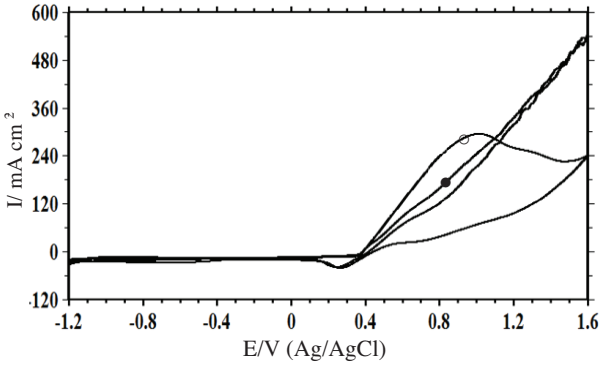

Figure 6. Effect of the MWNTs on the electrooxidation of 1.00 M methanol in 1.00 M KOH at the Ni@MWNTs (○) and Ni-C (●) electrodes at 298 K.

2.4. Effect of the scan rate on methanol electrooxidation

The cyclic voltammograms shown in Figure 7a were obtained with the Ni@MWNTs catalyst in 1.00 M methanol containing 1.00 M KOH solution at different scan rates (250, 200, 150, 100, 75, 50, 25 mV s^{-1}). Oxidation peak current densities of the nickel redox couple increased with increasing scan rate. Hereby, potentials became more positive. In the backward scan, NiOOH species, which were formed in the MOR in the forward scan,[12] were reduced to $Ni(OH)_2$. Formation of NiOOH on the catalyst surface leads to methanol oxidation.[26] The redox reaction mechanism Ni(II)/Ni(III) can be written as[27]

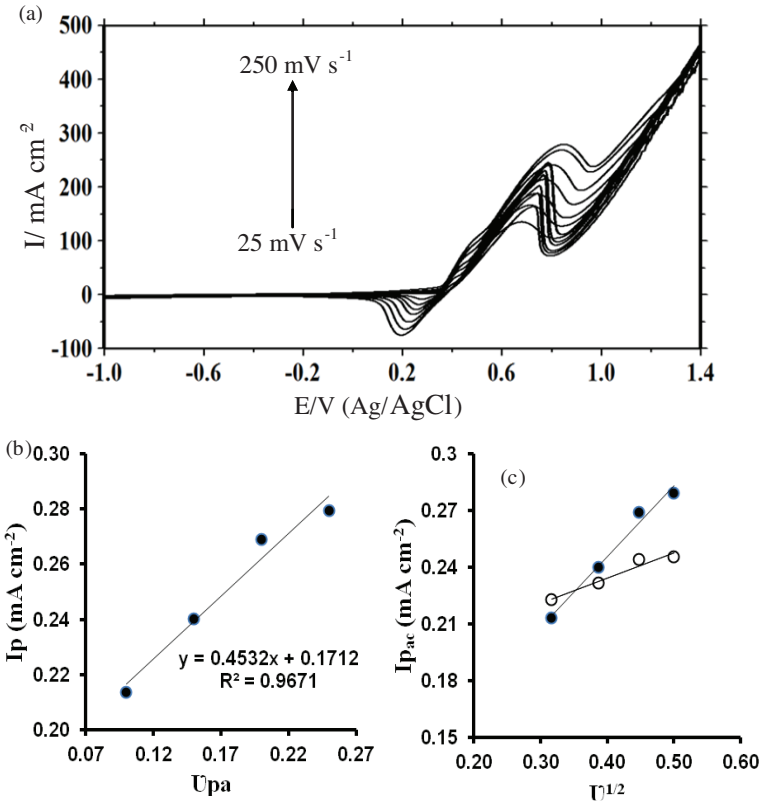

Figure 7. Effect of the different scan rates (250, 200, 150, 100, 75, 50, and 25 mV s^{-1}) on the electrooxidation of 1.00 M methanol in 1.00 M KOH at the Ni@MWNTs electrode at 298 K (a). Dependence of anodic peak current density during the forward scan on anodic peak potentials (b). Dependence of anodic (●) and cathodic (○) peak current densities during the forward and backward scan on the square roots of scan rate (c).

$$Ni + 2OH^- \rightleftharpoons Ni(OH)_2 + 2e^- \tag{1}$$

$$Ni(OH)_2 + OH^- \rightleftharpoons NiO(OH) + H_2O + e^- \tag{2}$$

As seen in Figure 7b, the oxidation peak current densities changed linearly from 25 to 75 mV s^{-1} scan rates. The surface coverage was calculated from the slope of the curve using the following equation:[28]

$$lp = \left(\frac{n^2F^2A\Lambda\Gamma}{4RT}\right)\chi\nu \tag{3}$$

where Ip, A, and Γ are anodic peak current density, electrode surface area, and surface coverage of the redox species, respectively. The surface coverage is approximately 6.01 × 10^{-9} and 1.46 × 10^{-8} mol cm^{-2} for Ni@MWNTs and C-Ni, respectively. Figure 7c shows the dependence of cathodic and anodic peak current densities on the square root of the scan rate. The linear curves indicate that the MOR is processing with diffusion control at the Ni@MWNTs electrode. The process of methanol oxidation is given as follows:[29,30]

$$CH_3OH_{aq} + NiOOH \xrightarrow{red.} C{\cdot}H_2OH_{ads} + Ni(OH)_2 \tag{4}$$

$$C{\cdot}H_2OH_{ads} + H_2O \xrightarrow{fast} HCOOH + 3e^- + 3H^+ \tag{5}$$

or

$$C{\cdot}H_2OH_{ads} + 3NiOOH + H_2O \xrightarrow{fast} HCOOH + 3Ni(OH)_2 \quad (6)$$

$$CHOOH \rightarrow CO_2 + 2H^+ + 2e^- \quad (7)$$

2.5. Effect of concentration on methanol electrooxidation

Figure 8a shows the dependence of concentration on methanol electrooxidation at the Ni@MWNTs catalyst at 100 mV s^{-1} scan rate. Peak current densities were 302.8 mA cm^{-2} and 7.35 mA cm^{-2} on electrooxidation of 1.00 M and 0.10 M methanol, respectively. As seen in Figure 8b, oxidation peak current densities increased with increasing methanol concentration because more methanol molecules penetrated into the catalyst surface for oxidation. Therefore, potentials shifted to a more positive region.

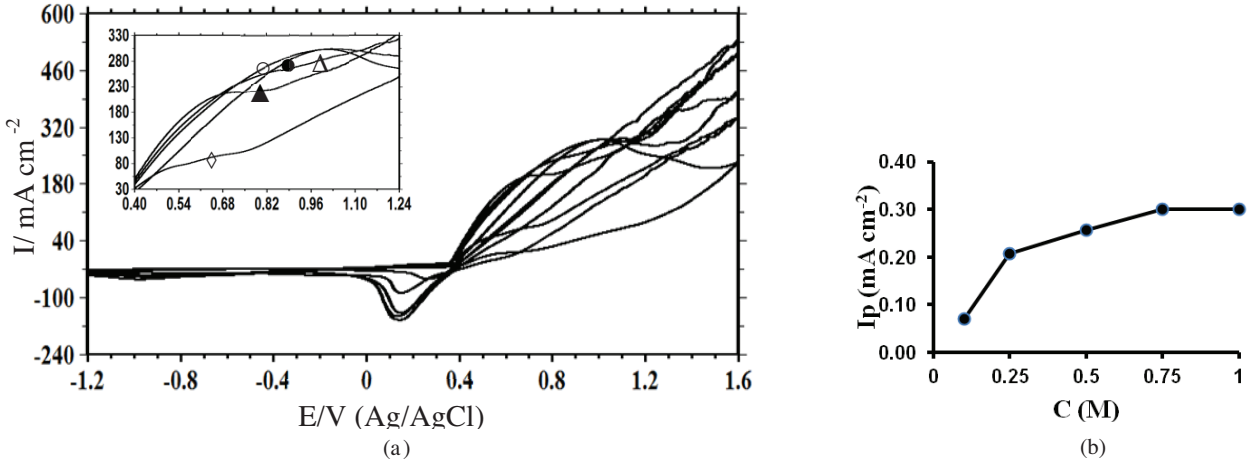

(a) (b)

Figure 8. Effect of the different concentrations of methanol ((●) 1.00 M, (○) 0.75 M, (Δ) 0.50 M, (▲) 0.25 M, (◇) 0.10 M) in 1.00 M KOH at Ni@MWNTs electrode at 298 K (scan rate υ: 100 mV s^{-1}) (a). Concentration–Ipa curve obtained on Ni@MWNTs electrode at 100 mV s^{-1} scan rate (b).

2.6. Effect of temperature on methanol electrooxidation

Figure 9 shows the effect of different temperatures on the electrooxidation of methanol at the Ni@MWNTs catalyst at 100 mV s^{-1}. Generally, reaction rates accelerate with increasing temperature. As seen in Figure 9a, oxidation current density rose with the rising temperature, which shows the acceleration of the electrochemical reaction. The highest oxidation peak current density was obtained at 318 K. It was not studied above 318 K because of the boiling temperature of methanol. Activation energies of the MOR at the Ni@MWNTs catalyst were calculated (Figure 9b).

The effect of different temperatures on the electrooxidation of methanol at the C-Ni catalyst at 100 mV s^{-1} is shown in Figure 10a. As seen in Figures 9 and 10, the oxidation peak current density at the Ni@MWNTs catalyst is higher than that at the C-Ni catalyst at 100 mV s^{-1}. Activation energies of the methanol electrooxidation reaction at the Ni@MWNTs and C-Ni catalysts (Figure 10b) were calculated with the Arrhenius equation as follows:

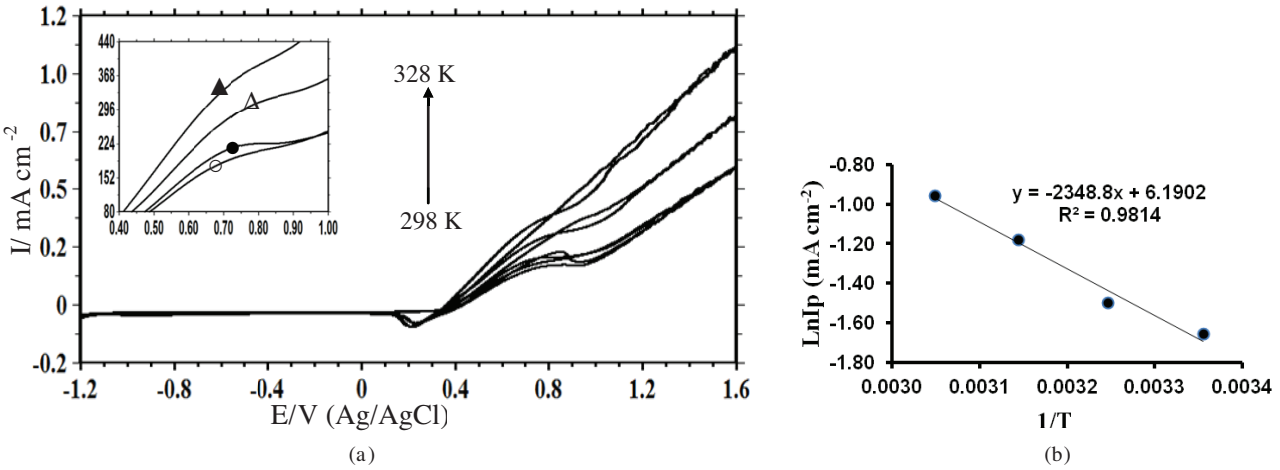

(a) (b)

Figure 9. Effect of the different temperatures (298 (○), 308 (●), 318 (Δ), 328 (▲) K) on the electrooxidation of 1.00 M methanol in 1.00 M KOH (scan rate υ: 100 mV s^{-1}) at the Ni@MWNTs electrode (a). 1/T – ln Ip curve obtained in 1.00 M KOH solution containing 1.00 M methanol on Ni@MWNTs electrode at 100 mV s^{-1} scan rate (b).

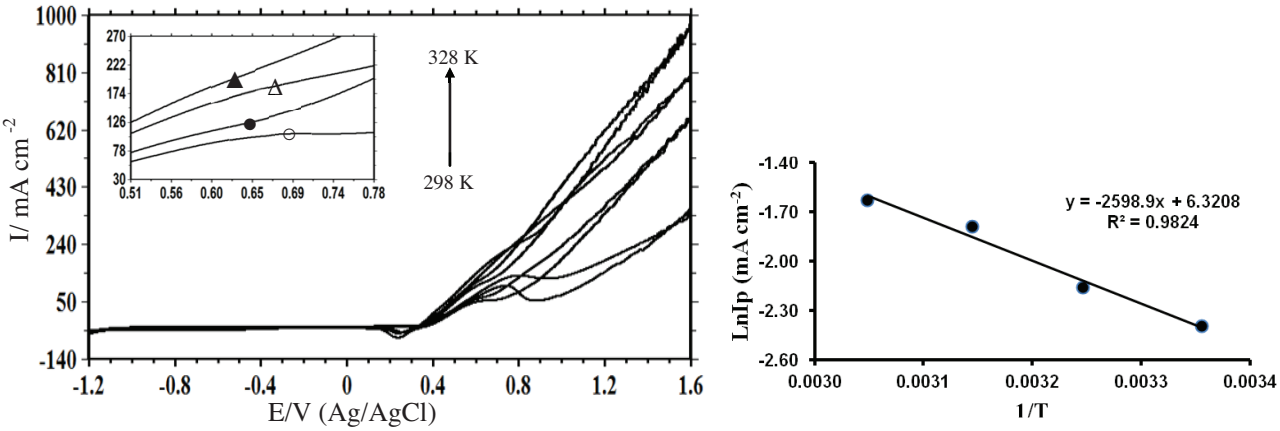

(a) (b)

Figure 10. Effect of the different temperatures (298 (◯), 308 (●), 318 (Δ), 328 (▲) K) on the electrooxidation of 1.00 M methanol in 1.00 M KOH (scan rate υ: 100 mV s^{-1}) at the Ni-C electrode (a). 1/T – ln Ip curve obtained in 1.00 M KOH solution containing 1.00 M methanol on Ni-C electrode at 100 mV s^{-1} scan rate (b).

$$\ln Ip = \ln A - Ea/RT, \tag{8}$$

where Ip, Ea, T, and A stand for peak current density, activation energy, temperature, and constant of Arrhenius, respectively. The activation energies are 19.52 and 21.61 kJ/mol for the Ni@MWNTs and C-Ni catalysts, respectively. The value of activation energy (Ea) of the MOR for the Ni@MWNT catalyst (19.52 kJ/mol) is quite smaller when compared to the literature data on Ea, which are prepared by Pt, Pd, Ru, and Ag catalysts in the range ∼40–60 kJ/mol....[31−34] On the other hand, similar Ea values were obtained from the literature for nickel catalysts.[35,36] The smaller activation energy indicates that using Ni@MWNTs as electrocatalysts makes the charge transfer process faster compared with the other three electrodes.

2.7. Chronoamperometric measurements

The electrocatalytic stability was measured at 3600 s, 298 K, and 0.60 V in 1.00 M KOH + 1.00 M methanol using chronoamperometry as shown in Figure 11. Chronoamperograms of C/MWNTs and C electrodes were obtained in order to compare them with nickel-deposited electrodes. Current densities of C and C/MWNTs electrodes were very close to each other and they stayed stable for 3600 s. At the beginning, current density decreased quickly at the Ni@MWNTs catalyst but a few seconds later it became stable. Current density decreased because the catalyst surface was poisoned by intermediate CO species. As a result, the activity of the catalyst was diminished.[37] As seen in Figure 11, the highest oxidation current density was achieved with the Ni@MWNTs catalyst. At 3600 s, this catalyst was more stable than the other three electrodes.

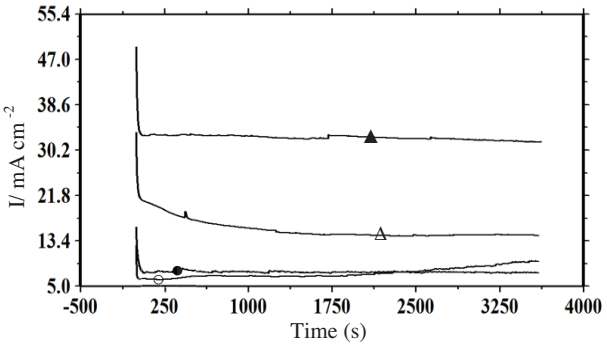

Figure 11. Chronoamperometric curves recorded in a 1.00 M methanol in 1.00 M KOH solution at E = 0.60 V vs. Ag/AgCl for Ni@MWNTs (▲), C-Ni (Δ), C/MWNTs (●), and C (○) electrodes.

3. Experimental

3.1. Preparation of electrodes

A graphite rod of length 5 cm was cut. One side was drilled and connected with copper wire to attain electrical conductivity. The graphite rod was immersed in polyester. The other side, with a surface area of 0.283 cm^2, was abraded with waterproof emery paper (grain size 150–1200), then washed with distilled water, scoured with acetone, and once again washed with distilled water. This process was repeated for each experiment. The electrodeposition was studied using the three-electrode technique, at room temperature and with a constant current. The bath solution was stirred nonstop using a magnetic stirrer. The counter and reference electrodes were a nickel sheet and a Ag/AgCl electrode, respectively.

(a) Preparation of C-Ni: The graphite electrodes were immersed in a nickel bath solution that had the composition of 30% $NiSO_4 \cdot 6H_2O$, 1.00% $NiCl_2 \cdot 6H_2O$, 1.25% H_3BO_3 (wt%). The current density of 100 mA cm^{-2} was applied to electrodeposition at different times (50, 80, 100, 200, 300 s) at 298 K. After these steps, the catalysts were flushed with distilled water to remove undesired particles from their surfaces.

(b) Preparation of Ni-deposited C/MWNTs: MWNTs are inert against chemical and electrochemical reactions. For activation, the MWNTs were ultrasonically treated with HNO_3 for 6 h at 298 K. After this process, a functional group with oxygen formed a MWNTs-graphite bond. Acidic MWNTs were filtered and mixed in acetone to form a suspension. Then 40 μL of the suspension was injected onto the surface of each working electrode to prepare C/MWNTs electrodes. The electrodes were inverted in a nickel bath

solution and a current density of 100 mA cm^{-2} was applied to the electrolysis at different times (50, 80, 100, 200, 300 s) and at 298 K to prepare the Ni@MWNTs catalyst.

Cyclic voltammetry and chronoamperometry (CA) measurements were performed with the three electrode technique using a CHI 608 D Electrochemical Analyzer (Serial: R0635) under computer control. A platinum plate (with a surface area of 2 cm^2) and a Ag/AgCl electrode were used as the counter and the reference electrodes, respectively. Cyclic voltammograms were obtained at different scan rates, temperatures and concentrations of methanol. Chronoamperometry measurements were performed at a constant potential. The electrochemical analyses were done in 1.00 M CH_3OH + 1.00 M KOH solution. The solution temperature was thermostatically controlled by a Nuve BS 302 type thermostat. All chemicals used were of analytical or chemical grade purity. All test solutions and catalysts were prepared freshly for each experiment. Every experiment was repeated at least three times. Energy dispersive X-ray (EDX) spectroscopy analysis was used to determine the chemical composition of the catalysts. Scanning electron microscopy (SEM - Carl Zeiss Leo 440 SEM instrument) took surface images at high vacuum and 20 kV EHT. Atomic force microscopy (AFM) showed the mean roughness of catalysts.

4. Conclusions

A Ni@MWNTs catalyst was prepared and tested in the methanol oxidation process for potential use as the anode catalyst of DMFCs. The prepared Ni@MWNTs catalyst was characterized using cyclic voltammetry, SEM, EDX, and AFM. The optimum deposition time was selected as 80 s. The electrooxidation ability of methanol was raised by using the Ni@MWNTs with a large specific surface area, synergistic combination, and high surface porosity. The activation energy of the Ni@MWNTs was calculated as 19.52 kJ/mol. The small activation energy supports our thesis that the Ni@MWNTs catalyst is a good anode in DMFCs. As a result of all the experiments, the Ni@MWNTs catalyst could be preferred for use in DMFCs.

Acknowledgments

The authors are greatly thankful to Çukurova University Research Fund for its financial support (Project Number: FEF2010YL54) and Osmaniye Korkut Ata University. The authors also would also like to thank Kirsi Ekroos for language support.

References

1. Cairns, E. J.; Albertus, P. *Annu. Rev. Chem. Biomol. Eng.* **2010**, *1*, 299–320.
2. Padbury, R.; Zhang, X. *J. Power Sources* **2011**, *196*, 4436–4444.
3. Nouralishahi, A.; Khodadadi, A. A.; Mortazavi, Y.; Rashidi, A.; Choolaei, M. *Electrochim. Acta* **2014**, *147*, 192–200.
4. Ahmadi, R.; Amini, M. K.; Bennett, J. C. *J. Catal.* **2012**, *292*, 81–89.
5. Barakat, N. A. M.; Motlak, M.; Elzatahry, A. A.; Khalil, K. A.; Abdelghani, E. A. M. *Int. J. Hydrogen Energy* **2014**, *39*, 305–316.
6. Raoof, J.; Golikand, A.; Baghayeri, M. *J. Solid State Electrochem.* **2010**, *14*, 817–822.
7. Wen, T.-C.; Lin, S.-M.; Tsai, J.-M. *J. Appl. Electrochem.* **1994**, *24*, 233–238.
8. Liu, Z.; Li, Z.; Wang, F.; Liu, J.; Ji, J.; Wang, J.; Wang, W.; Qin, S.; Zhang, L. *Mater. Lett.* **2011**, *65*, 3396–3398.
9. Spinner, N.; Mustain, W. E. *Electrochim. Acta* **2011**, *56*, 5656–5666.

10. Döner, A.; Telli, E.; Kardaş, G. *J. Power Sources* **2012**, *205*, 71–79.
11. El-Shafei, A. *J. Electroanal. Chem.* **1999**, *471*, 89–95.
12. Zhang, S.; Zheng, Y.; Yuan, L.; Wang, X.; Zhao, L. *Int. J. Hydrogen Energy* **2014**, *39*, 3100–3108.
13. Carmo, M.; Paganin, V.; Rosolen, J.; Gonzalez, E. *J. Power Sources* **2005**, *142*, 169–176.
14. Dicks, A. L. *J. Power Sources* **2006**, *156*, 128–141.
15. Jin, G.-P.; Ding, Y.-F.; Zheng, P.-P. *J. Power Sources* **2007**, *166*, 80–86.
16. Wu, G.; Xu, B.-Q. *J. Power Sources* **2007**, *174*, 148–158.
17. Rajalakshmi, N.; Ryu, H.; Shaijumon, M.; Ramaprabhu, S. *J. Power Sources* **2005**, *140*, 250–257.
18. Li, L.; Wu, G.; Xu, B.-Q. *Carbon* **2006**, *44*, 2973–2983.
19. Chen, C.-C.; Chen, C.-F.; Chen, C.-M.; Chuang, F.-T. *Electrochem. Commun.* **2007**, *9*, 159–163.
20. Ocampo, A.; Miranda-Hernandez, M.; Morgado, J.; Montoya, J.; Sebastian, P. *J. Power Sources* **2006**, *160*, 915–924.
21. Prabhuram, J.; Zhao, T.; Tang, Z.; Chen, R.; Liang, Z. *J. Phys. Chem. B.* **2006**, *110*, 5245-5252.
22. Shamsipur, M.; Najafi, M.; Milani Hosseini, M.-R. *J. Appl. Electrochem.* **2013**, *43*, 1027–1033.
23. Vaze, A.; Sawant, S.; Pangarkar, V. *J. Appl. Electrochem.* **1997**, *27*, 584–588.
24. Liu, S.-J. *Electrochim. Acta* **2004**, *49*, 3235–3241.
25. Taraszewska, J.; Rosłonek, G. *J. Electroanal. Chem.* **1994**, *364*, 209–213.
26. Yang, Y. *Bull. Mater. Sci.* **2012**, *35*, 513-517.
27. El-Shafei, A. A. *J. Electroanal. Chem.* **1999**, *471*, 89–95.
28. Bard, A. J.; Faulkner, L. R. *Electrochemical Methods: Fundamentals and Applications*; Wiley: Austin, TX, USA, 2001.
29. Frackowiak, E.; Gautier, S.; Gaucher, H.; Bonnamy, S.; Beguin, F. *Carbon* **1999**, *37*, 61–69.
30. Kowal, A.; Port, S. N.; Nichols, R. J. *Catal. Today* **1997**, *38*, 483–492.
31. Batista, E.; Hoster, H.; Iwasita, T. *J. Electroanal. Chem.* **2003**, *554*, 265–271.
32. Lamy, C.; Guenot, B.; Cretin, M.; Pourcelly, G. *Electrochim. Acta* 2015; DOI: 10.1016/j.electacta.2015.02.069.
33. Dubau, L.; Coutanceau, C.; Garnier, E.; Léger, J. M.; Lamy, C. *J. Appl. Electrochem.* **2003**, *33*, 419–429.
34. Wang, Y.; Sheng, Z. M.; Yang, H.; Jiang, S. P.; Li, C. M. *Int. J. Hydrogen Energy* **2010**, *35*, 10087–10093.
35. Telli, E.; Döner, A.; Kardaş, G. *Electrochim. Acta* **2013**, *107*, 216–224.
36. Wang, W.; Liu, Y.; Dong, W.; Yang, Y.; Zhou, X.; Lei, Z. *Int. J. Hydrogen Energy* **2015**, *40*, 3892–3899.
37. Antolini, E. *Appl. Catal. B-Environ.* **2007**, *74*, 337–350.